We've shown that no additional info on topography is needed to infer deformation if three radar passes are available. We simply calculation the ratio of the $B_{\perp}$'s and found the combined product

$$\phi' - \frac{B'_{\perp}}{B_{\perp}} \phi = -\frac{4\pi}{\lambda} \Delta\rho$$

Consider the baseline ratio in more detail:

$$\frac{B'_{\perp}}{B_{\perp}} = \frac{B' \sin(\theta - \alpha')}{B \sin(\theta - \alpha)}$$

Now, this ratio depends on θ, which in turn depends on topography. Once again we are limited by knowledge of the topography of a region. However, by making certain approximations it is possible to proceed quite nicely.

Let's correct the measured fringe patterns ϕ and ϕ' for the "flat-earth" correction, that is remove the phase pattern which would result from an earth surface devoid of topography. In that case we can calculate the look angle exactly, denoting it by θ_{flat}:

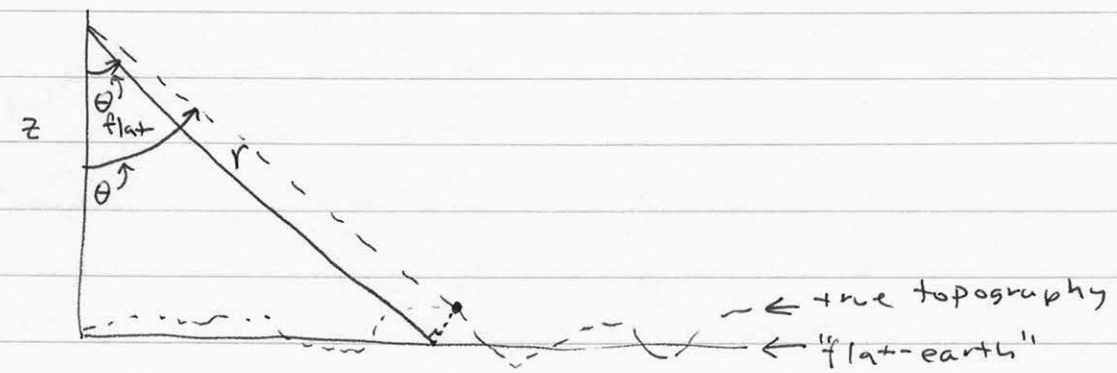

Define as ϕ_{flat} the phase after "flattening", or correction by the expected flat-earth fringe pattern. Using the same baseline length and orientation we have

$$\phi_{flat} = -\frac{4\pi}{\lambda}\left[B\sin(\theta-\alpha) - B\sin(\theta_{flat}-\alpha)\right]$$

$B_{\parallel}$ assuming topography

$B_{\parallel}$ in the case of no topography

Since $\theta_{flat} \approx \theta$, we can simplify the above expression using

$$\theta = \theta_{flat} + \delta\theta$$

$$\sin(\theta-\alpha) = \sin(\underset{flat}{\theta-\alpha} + \delta\theta)$$

$$\approx \sin(\theta_{flat}-\alpha) + \cos(\theta_{flat}-\alpha)\,\delta\theta$$

so that

$$\phi_{flat} = \frac{-4\pi}{\lambda} B\cos(\theta_{flat}-\alpha)\,\delta\theta$$

Under these approximations the flattened phase is proportional now to the perpendicular component of the baseline and to the angular topographic distortion $\delta\theta$ directly. So now when we form the ratio

$$\frac{\phi'_{flat}}{\phi_{flat}} = \frac{\frac{-4\pi}{\lambda} B'\cos(\theta_{flat}-\alpha')\,\delta\theta}{\frac{-4\pi}{\lambda} B\cos(\theta_{flat}-\alpha)\,\delta\theta} = \frac{B'_{\perp}}{B_{\perp}}$$

which doesn't depend on topography at all.

Hence we can restate the differential phase equation in terms of the flattened phase

$$\phi'_{flat} - \frac{B'_\perp}{B_\perp}\phi_{flat} = -\frac{4\pi}{\lambda}\Delta\rho$$

and now there is no topographic dependence at all. Hence we scale flattened interferograms by the ratio of the perpendicular baselines rather than scaling unflattened interferograms by parallel components of the baselines.

Sensitivity of deformation maps

Now consider the sensitivity of our deformation measurements as compared to topographic measurements. Begin by determining the sensitivity of the phase measurement ϕ to height and deformation in our total phase equation

$$\phi = -\frac{4\pi}{\lambda}\left[B\sin(\theta-\alpha) + \Delta\rho\right]$$

We've done $\frac{d\phi}{dz}$ for the sensitivity many times now:

$$\frac{d\phi}{dz} = -\frac{4\pi B}{\lambda r}\frac{\cos(\theta-\alpha)}{\sin\theta}$$

Add to this

$$\frac{d\phi}{d\Delta\rho} = \frac{-4\pi}{\lambda}$$

Because usually $\frac{B}{r} << 1$, our interferogram will be very much

more sensitive to small changes in deformation rather than topography. We can illustrate this by looking at values for typical ERS geometries:

$r = 800$ km

$\theta = 23°$

$\alpha = 0°$

$B = 200$ m

$\lambda = 6$ cm

$$\frac{d\phi}{dz} = \frac{-4\pi \cdot 200}{0.06 \cdot 800 \times 10^3} \cdot \frac{\cos 23°}{\sin 23°}$$

$$= -0.123 \text{ rad/m} = -7°/\text{m}$$

Hence a 1 m topography signature results in 7° of interferometric phase, near the limit of detectability. Thus meter-scale topographic accuracy is possible.

How about for deformation?

$$\frac{d\phi}{d\Delta\rho} = \frac{-4\pi}{0.06}$$

$$= -209 \text{ rad/m} = 11,938°/\text{m}$$

A 1m deformation signature gives nearly 12000° of phase, about 30 cycles. Hence a very small amount of deformation is detectable with interferometric techniques.

This argument should help illustrate that deformation enters into the interferogram phase in a fundamentally different way than does topography. In the topographic case a position is scaled by a ratio of about $\frac{B}{r}$ before adding to the phase, while for deformation it enters directly.

Therefore deformation measurements are $\frac{r}{B}$ times more sensitive than simple differencing of topography at two different times would suggest.

A case example - Landers earthquake

We will illustrate the deformation measurement by looking in more detail at the magnitude 7.3 earthquake centered near Landers, CA, in June 1992. This was the first earthquake studied in detail by radar interferometry.

The data for this study were acquired by ERS-1 on April 24, July 3, and August 7, 1992. The earthquake occured on June 28.

We can form several interferograms from these data, consider one pair from the April and August images, and one from the July and August images.

The July-August pair will form an interferogram dominated by topography since no other large motions occured during this period. But the April-August pair span the large earthquake, and we would expect a significant ϕ_{eq} term in our phase expression.

We could also use the April-July pair to form an earthquake-containing interferogram. However, this pair has a

very large baseline associated with it, and the high fringe rate makes it difficult to read the phase values accurately. Our baseline data are as follows:

Pair	B	α	$B_{\parallel}$	$B_{\perp}$
April - August	146	152	110	96
July - August	503	175	220	452

We can sketch the locations in the sky as follows:

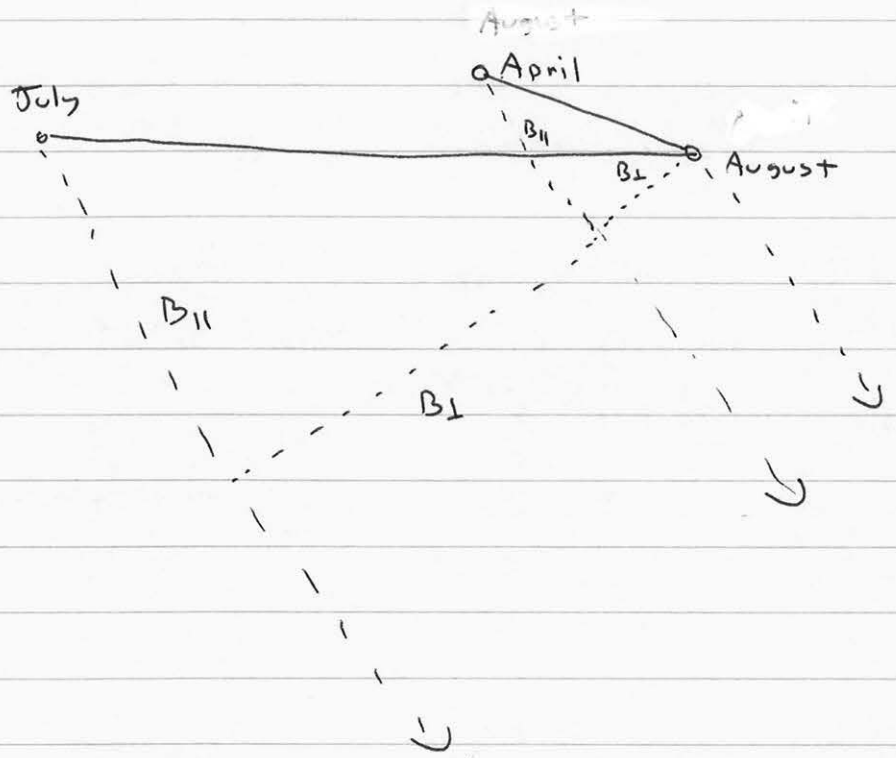

We are stuck with the long-baseline July-August pair since it is the only one with no deformation. We choose April-August over April-July because it has a shorter baseline.

When we examine these two interferograms, we expect a

much higher fringe rate for July-August than for April-August, and this is indeed what we see.

We also would expect a higher correlation in the shorter baseline pair. Recall how we modeled correlation as a function of baseline length:

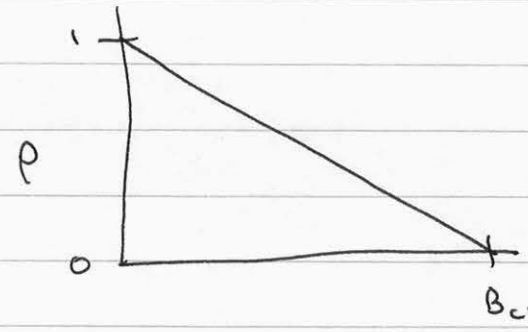

It fell off linearly with baseline to a maximum baseline of $B_{critical}$. Evaluating $B_{critical}$ for ERS:

$$B_{critical} = \frac{\lambda r}{2\cos\theta \delta y}$$

$$= \frac{6\text{ cm} \cdot 800\text{ km}}{2 \cdot \cos 23^\circ \cdot 25\text{ m}}$$

$$\approx 1050\text{ m}$$

As $B_\perp$ for July-August is 452 m, the correlation ought to be decreased by about half, as we observe.

→ Viewgraphs in class depict these and the resulting 3-pass deformation interferogram ←

In the case at Landers we were fortunate to also have GPS satellite measurements of the deformation available. We might compare the radar interferometer measurements with the GPS data.

Now, note that while the GPS measurements are vector quantities the radar only is sensitive to motion in the line of sight of the radar antenna. Thus only one component is measured in the interferogram. To compare them we calculate the dot product of the GPS measurement with a unit vector in the radar line of sight. The results look like this:

Table 2. Comparison of Radar and GPS Motion Estimates

Site	Latitude, deg	Longitude, deg	Horizontal Displacement for Observed Radar Motion, cm	GPS Vector in Radar Direction, cm	Difference, cm
6052	34.52	−116.84	47.8	33.2	14.6
6056	34.37	−116.65	18.1	21.9	−3.8
7000	34.68	−116.72	36.8	91.1	−54.3
7001	34.56	−116.47	−37.1	−70.2	33.1
HECT	34.79	−116.42	9.7	−5.2	14.9
LAZY	34.34	−116.51	62.9	49.4	13.5
LUCS	34.44	−116.88	26.4	20.7	5.7
POIN	34.45	−117.07	13.4	9.5	3.9
SOAP	34.90	−116.98	12.3	1.7	10.6
STIM	34.54	−117.24	7.8	7.4	0.4
FLASH	34.82	−117.02	14.1	12.1	2.0
HARVARD	34.94	−116.67	7.5	−0.4	7.9
BOULDER	34.51	−116.56	176.1	210.8	−34.7
FRY	34.50	−116.72	66.0	74.6	−8.6
MEANS	34.41	−116.55	82.2	69.8	12.4
OLD WOMN	34.39	−116.75	25.0	17.1	7.9
ORD	34.68	−116.81	44.4	48.3	−3.9
ROCK	34.54	−116.77	63.9	69.1	−5.2

where we have related a radar horizontal displacent estimate to slant range measurements by the usual

$$\Delta y = \frac{\Delta \rho}{\sin \theta}$$

If we plot both radar and GPS displacements we see clearly the difference between vector and scalar measurements:

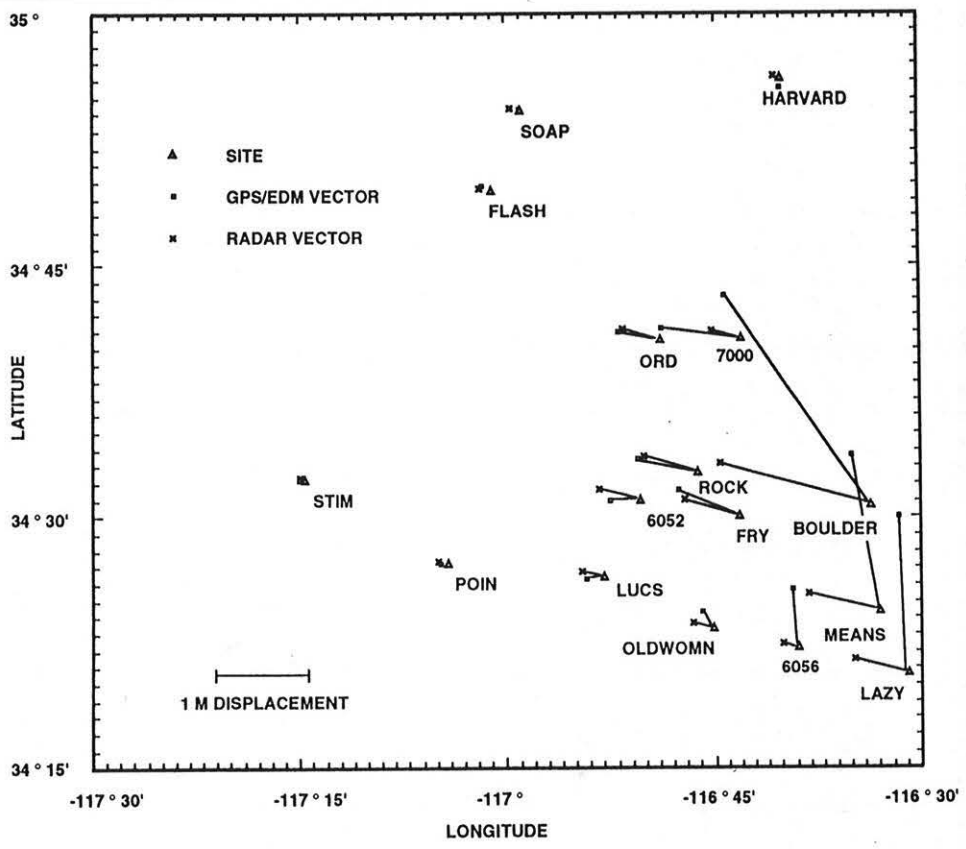

Figure 4. Displacement vectors as measured by GPS/EDM data and by radar interferometry. Each GPS or EDM site is denoted by a triangle, and a vector ending with a square (GPS/EDM measurement) and a vector ending with a cross (radar measurement) are shown in the direction of motion. Note that for the radar case only the component in the radar line of sight direction is determined and thus all measurements are parallel. Vectors are correlated at 0.96 level and show that radar and field surveys are measuring similar phenomena.

We can also look at the statistical correlation (not interferogram correlation) and see that the two sets of measurements are 96% correlated:

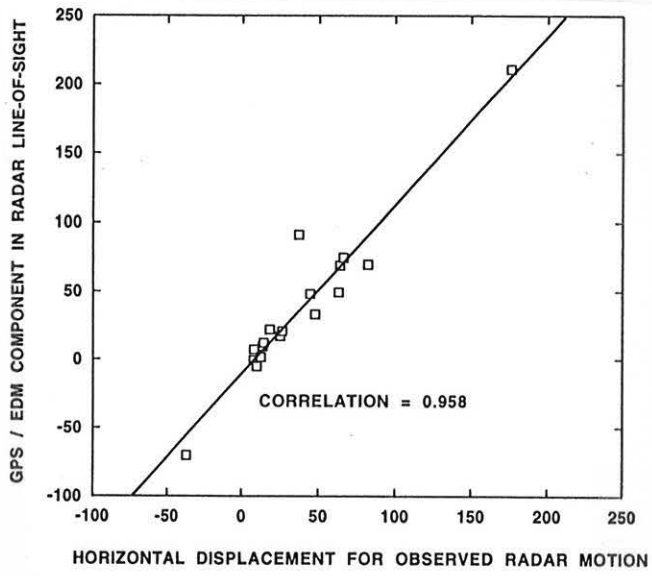

Figure 3. Scatter plot of displacement measurements with GPS/EDM data on vertical axis and radar measurements on horizontal axis. The correlation of the data sets is 0.96, however a slight bias is observed as the slope of the line is not 1.